Weighted Metapath Projection for SIR Epidemic Modeling on Tripartite Networks

João Gabriel Melo Barbirato[1], **Alneu de Andrade Lopes**[1]

[1]Institute of Mathematics and Computer Science – University of São Paulo (USP)

jgmbarbirato@usp.br, alneu@icmc.usp.br

Abstract. *Diffusion models are a set of rules that describe the dynamics of information spread. Despite many proposed methods, few have extended these structures to tripartite networks. To address this gap, this work proposes an SIR model for tripartite networks by projecting the tripartite graph onto a weighted unipartite graph with a metapath. After testing on 150 synthetic small networks, results show that an adaptive projection significantly outperforms both the global and naive approaches in node rank correlation with ODE output. A spectral analysis shows that all three approaches agree on identifying influential spreaders. An exploratory comparison of epidemic thresholds suggests differences across methods, though this result may be biased by graph size.*

1. Introduction

Diffusion processes on networks describe how a state (information, a behavior, or an infection) propagates from a subset of nodes to the rest of a population through a set of rules or equations. In complex networks, node-to-node propagation is also dictated by the edges connecting them [Newman 2018]. Among diffusion models, compartmental epidemic models such as Susceptible-Infected-Recovered (SIR) remain a cornerstone both for representing real epidemic processes and as a generic framework for spreading phenomena more broadly, since they capture the topology-dependence of large-scale outbreaks through a small number of interpretable parameters and a system of coupled ordinary differential equations (ODEs) [Kermack and McKendrick 1927].

Classical compartmental models on networks frequently assume a single-type, homogeneous population and assume that any adjacent infected node can infect it, regardless of type. However, spreading occurs across multiple structurally distinct categories rather than within a single category in many real systems, and several works have proposed bipartite extensions of compartmental ODE models to capture this. [Gómez-Gardeñes et al. 2008] introduces a method for a compartmental model over bipartite scale-free graphs representing heterosexual contact networks, with separate male and female compartments and degree-class stratification used to derive the epidemic threshold. [Bisanzio et al. 2010] models vector-borne disease transmission as spreading over a bipartite host–vector network, showing that the epidemic threshold is governed by the degree distributions of the two node categories rather than by population size alone. More recently, [Takko et al. 2023] represents human mobility during the COVID-19 pandemic as a bipartite network linking populations to the locations they visit, and derives a weighted one-mode projection of this structure to estimate exposure between populations. Therefore, the work indicates that a weighted unipartite projection can stand in for a bipartite contact structure for certain modeling purposes.

These studies indicate that partitioning a population into structurally separate categories changes diffusion dynamics, and that a bipartite formulation is more true to the underlying contact process than compacting it into a single homogeneous population. Moving beyond the bipartite situation, many real-world systems ubiquitously divide into three or more semantically distinct classes of entities. Heterogeneous information networks studied extensively in the data mining literature — e.g., DBLP (authors, papers, venues), ACM (papers, authors, subjects), IMDB (movies, actors, directors), and AMiner (papers, authors, venues) — are routinely represented as multipartite networks precisely because a two-mode decomposition discards relevant structure. To the best of our knowledge, compartmental epidemic models on networks have rarely been studied past the bipartite case. [Santos et al. 2013] generalizes SIS dynamics to a multipartite network, but hasn't tackled unipartite projections. [Lee et al. 2021] showed that unipartite projection snapshots from temporal networks can lose information needed to reproduce multipartite dynamics, but hasn't tackled weighting the projection.

In that sense, each additional node category introduces new compartments and new pairwise cross-infection terms, and, once degree heterogeneity across categories is taken into account, additional degree-category stratifications grow combinatorially with the number of layers k. This becomes costly to calibrate and to interpret, and limits a full multipartite ODE system to small networks. A common strategy in network science for handling multipartite structure is to project the multipartite graph onto a unipartite graph, such as a co-authorship network derived from a bipartite author–paper graph, or a weighted network derived from a bipartite mobility graph [Takko et al. 2023]. These projections simplify the topology and are intended to preserve more of the original relational structure than an unweighted projection would when edges are weighted by the strength of shared connections. Thus, there is potential for weighted projections to maintain both simplicity and dynamical fidelity.

Therefore, this work aims to address whether a weighted unipartite projection of a tripartite contact structure can reproduce epidemic dynamics of the corresponding full tripartite compartmental ODE system, and how this method preserves topology fidelity. This work's main contributions are: (I) a tripartite generalization of the bipartite SIR compartment ODE system, extending the cross-infection structure to three interacting node layers; (II) a framework which consists on projecting the tripartite graph onto a single weighted unipartite graph and simulating a standard single-population SIR model on it; (III) three methods of weighting the unipartite graph; and (IV) the evaluation on how closely the projection-based SIR reproduces the dynamics of the full tripartite ODE system, correlating the two across 150 small synthetic tripartite networks. Our results show a trade-off between the naive unweighted projection, which best preserves the epidemic threshold, and the Adaptive layer-wise parameter weighted projection, which achieves significantly better node rank correlations with tripartite ODE. Both outperform the method that assigns a global parameter across all layers on different aspects.

The remainder of this paper is organized as follows. Section 2 reviews related work on the topics; Section 3 presents the tripartite SIR ODE formulation and the weighted projection method; Section 4 describes the experiment setup; Sections 5 and 6 show experiment results and their discussion, respectively. Lastly, Section 7 presents final considerations and conclusions.

2. Related works

Propagation models describe the spread function through a dynamic diffusion process driven by rules that vary across models, applications, and networks [Newman 2018]. Different propagation models propose different rules [Kermack and McKendrick 1927, Granovetter 1978, Kempe et al. 2003]. Among them, epidemic compartment models categorize nodes by the stage of a disease they are in. The main states include Susceptible (S), Infected (I), and Recovered (R). Thus, the Susceptible-Infected (SI), Susceptible-Infected-Susceptible (SIS), and Susceptible-Infected-Recovered (SIR) models stand out [Kermack and McKendrick 1927].

Regarding epidemic models on bipartite networks, [Gómez-Gardeñes et al. 2008] proposes a compartmental SIS model over bipartite scale-free graphs representing heterosexual contact networks. Each layer had separate compartments and model parameters. The authors concluded that a uniform-weighted projection, assuming a scale-free distribution, could not replicate the bipartite epidemic threshold. [Bisanzio et al. 2010] models a bipartite vector-borne disease transmission as a bipartite *host-vector* process. The work concludes that epidemic thresholds can vanish when the bipartite network is projected onto hosts, as the results show a long-tailed distribution. [Xu et al. 2025] extended the host-vector formulation with fractional dynamics validated with scale-free and random synthetic graphs. The work concludes that long-term memory systems provided by fractional-order models can contribute to epidemic prediction on a bipartite network, but it also assumes a well-mixed diffusion[1] and doesn't tackle a unipartite solution. Together, these works indicate that propagation between layers alone is insufficient to process the diffusion in the network.

Regarding multipartite epidemic models, [Santos et al. 2013] derives mean-field nonlinear differential equations to describe multi-virus epidemics over stochastic multipartite networks. The authors conclude that the proposed diffusion depends on connections between groups of nodes within the same layer. However, they assume a well-mixed system and haven't accounted for alleviating hub biases in the network propagation.

Regarding network projections and dynamical fidelity, [Takko et al. 2023] builds a bipartite population-location mobility network for COVID-19 to project an unipartite network. The authors showed that a weighted projection serves as a proxy for the bipartite graph, enabling novel topological analysis of the projected network. Although the weighting process is built on empirical data rather than the multipartite topology itself, the authors justify its use when projecting onto unipartite graphs. [Lee et al. 2021] compares transmission dynamics on temporal multipartite networks against uniformly-weighted time-aggregated unipartite projections. The authors conclude that these different structures show distinct outbreak sizes and trajectories. Consequently, neither work isolates how projecting and weighting determine diffusion fidelity, leaving an open question for further exploration.

3. Proposed method

Let $G(\{N_1, N_2, N_3\}, \{E_{1,2}, E_{2,3}, E_{1,3}\})$ be an undirected tripartite graph, where N_i is the set of nodes of the i-th layer and $E_{i,j}$ is the set of edges between layers i and

[1]Equal probability of each node being activated by any other.

j. Moreover, consider metapaths of size k as random walks restricted by a sequence $t_{n_1} \xrightarrow{t_{e_1}} t_{n_2} \xrightarrow{t_{e_2}} ... \xrightarrow{t_{e_k}} t_{n_{k+1}}$ of node types, where n_1, n_2, n_{k+1} are nodes and e_1, e_2, e_k are edges [Sun and Han 2012]. Our goal is to approximate the epidemic propagation on G by creating a unipartite projection of the first layer through weighting according to the metapath $N_1 \rightarrow N_2 \rightarrow N_3 \rightarrow N_2 \rightarrow N_1$, resulting in a weighted graph $G_{proj}(N_1, E_{proj})$[2].

To build a ground-truth deterministic method, we adapted the proposed bipartite SIS [Gómez-Gardeñes et al. 2008, Bisanzio et al. 2010, Xu et al. 2025] ODEs to tripartite SIR. The set of equations that describes the infected nodes is defined in Equation 1, which assumes a disease-free state[3] and contact approximated through adjacency [Pastor-Satorras and Vespignani 2001].

$$\begin{aligned} \frac{dI_1}{dt} &= \beta_{21} A_{12} I_2 - \gamma_1 I_1 \\ \frac{dI_2}{dt} &= \beta_{12} A_{12}^T I_1 + \beta_{32} A_{23} I_3 - \gamma_2 I_2 \\ \frac{dI_3}{dt} &= \beta_{23} A_{23}^T I_2 - \gamma_3 I_3 \end{aligned} \tag{1}$$

where A_{ij} is the bipartite adjacency matrix between layers i and j; β_{ij} is the infection rate of a node in layer i activates a node in layer j; γ_i is the recovery rate of a node in the i-th layer; and I_i is the infected node count in layer i.

Moreover, this work proposes the weighted metapath projection for the SIR[4] epidemic diffusion model. After projecting the network onto a unipartite graph, Equation 2 describes how the proposed method applies the standard SIR equation.

$$\frac{dI_1}{dt} = \beta_{proj} W I_1 - \gamma_{proj} I_1 \tag{2}$$

where β_{proj} is the infection rate in the projected network; γ_{proj} is the recovery rate; and W the proposed projected adjacency matrix. Furthermore, the proposed methods of calculating W are described in 3.1, 3.2, and 3.3.

3.1. Naive method

This method is a direct, uniformly weighted projection. Its behavior is described in Equation 3.

$$W_{naive} = A_{12} \cdot A_{23} \cdot A_{23}^T \cdot A_{12}^T \tag{3}$$

3.2. Global method

This method adjusts each layer in the metapath using a single tunable parameter (α) to compensate for the projection's structural bias. Inspired by the $L3$ index algorithm [Kovács et al. 2019], to alleviate the impact of hubs in different layers, we use each layer's degree centrality[5] with the tunable parameter, as described in Equation 4.

[2]Although G may contain $E_{1,3}$, our modeling assumes cross-partition diffusion occurs only through P2.

[3]Nodes are approximately all susceptible.

[4]We adopt SIR as a general-purpose diffusion abstraction due to its recovery mechanism.

[5]In this case, an edge count.

$$W_{global}(\alpha_{global}) = A_{12} \cdot D_2^{-\alpha_{global}} \cdot A_{23} \cdot D_3^{-\alpha_{global}} \cdot A_{23}^T \cdot D_2^{-\alpha_{global}} \cdot A_{12}^T \quad (4)$$

3.3. Adaptive method

This method also alleviates the impact of the layer-degree distribution within each layer of the metapath, now using two tunable parameters, α_2 and α_3, for layers 2 (the closer layer) and 3 (the furthest layer), respectively. This concept is defined in the Equation 5.

$$W_{adapt}(\alpha_2, \alpha_3) = A_{12} \cdot D_2^{-\alpha_2} \cdot A_{23} \cdot D_3^{-\alpha_3} \cdot A_{23}^T \cdot D_2^{-\alpha_2} \cdot A_{12}^T \quad (5)$$

4. Experiments

This section describes the elements of the conducted experiments to validate our proposal. Every code was written in Python[6], mostly using the following libraries: PyTorch[7], PyTorch Geometric[8], SciPy[9] and NetworkX[10]. Results and code are available publicly[11].

4.1. Dataset

We generated synthetic tripartite networks to conduct our experiment. To diversify graph topologies, we made it so every layer's node degree distribution would follow (1) the scale-free Barabàsi-Albert graph model, (2) the random Erdos-Renyi graph model, or (3) the clustered Stochastic Block graph model. Therefore, we generate 50 graphs for each model, henceforth referred to as graph classes.

Nonetheless, each graph has a range of $(30, 60)$ nodes in each layer. Scale-free had a range of $(1.5, 3.0)$ edges attached to new nodes, random graphs had a range of $(0.01, 0.075)$ probability of creating an edge between nodes, and clustered graphs had at most 3 clusters each layer. These parameters were stochastically chosen to ensure a variety of topologies across the three graph classes.

4.2. Diffusion parameters

For ODE systems, we assumed a recovery rate of $\gamma_i = 0.05$ for each layer i. Then, we calculated the infection rate β_{ij} of a node i activate j, as the basic reproductive number $R_0 = \frac{\beta}{\gamma}$ can be assumed as the largest eigenvector[12] [Castillo-Garsow and Castillo-Chavez 2020]. Moreover, ODE resolution were computed with the Runge–Kutta–Fehlberg approximation method. For stochastic simulations on the unipartite graph described in 4.3.2, we also assumed the same rules for γ and β. To calculate weighting matrices, we exhaustively fitted the best α values through grid-search across 20 points in the $(0, 1)$ range. Moreover, we established 100 simulations per node to measure each node's recovery cascade.

[6]Available at: `https://www.python.org/`. Last visited: June 2026.

[7]Available at: `https://pytorch.org/`. Last visited: June 2026.

[8]Available at: `https://pytorch-geometric.readthedocs.io/en/latest/`. Last visited: June 2026.

[9]Available at: `https://scipy.org/`. Last visited: June 2026.

[10]Available at: `https://networkx.org/`. Last visited: June 2026.

[11]`https://github.com/joaobarbirato/wmsir`

[12]Thus, $\beta \approx \lambda\gamma$, with λ as the largest eigenvector.

4.3. Evaluation

This section describes the evaluation of the proposed methods in this work. In 4.3.1, we present qualitative measures, as well as quantitative measures in 4.3.2.

4.3.1. Qualitative analysis

To further understand the impact of edge existence, in addition to following node distributions, we measure graph density[13] both globally and between specific pairs of layers, as described in Table 1.

Table 1. Density measures used in this work. Consider $|E|$ the number of total edges in the graph; $|E_{ij}|$ the number of edges between layers i and j; and $|N_i|$ the number of nodes in layer i.

Density	Equation
Homogeneous density	$d_{homo} = \frac{\|E\|}{\|N_1\|\|N_2\|+\|N_1\|\|N_3\|+\|N_2\|\|N_3\|}$
Bipartite density	$d_{nm} = \frac{\|E_{nm}\|}{\|N_n\|\|N_m\|}$
Tripartite density	$d_{tri} = \frac{\|E_{12}\|+\|E_{23}\|}{\|N_1\|\|N_2\|+\|N_2\|\|N_3\|}$

Moreover, to ensure that the diffusion process in the unipartite projection approximates the original, we conducted two fidelity evaluations of network eigenvalues and eigenvectors. Because epidemic diffusion is tied to these parameters, the higher the correlation, the greater the fidelity of the model in reproducing epidemic behavior in the network using the projection.

- **Eigenvector fidelity –** Pearson correlation between the leading eigenvectors of the projected weighted and full tripartite contact matrices. Its goal is to show if the projection agrees on important spreaders;
- **Threshold fidelity –** the ratio of the projected graph's spectral radius to that of the full tripartite system, approximating R_0 preservation. Its goal is to show if the projection agrees with the epidemic threshold;

4.3.2. Quantitative analysis

To validate that our Adaptive projection accurately captures the system's epidemic potential, we employ a dynamic validation approach. We compare the node-level recovered node count from the full-system ODEs with the trajectory predicted by the projection, as this is what distinguishes SIR from SI and SIS. This prediction was conducted using Monte Carlo simulations, a widely used approach in influential node identification works [Wang et al. 2025, Zheng et al. 2025, Guo et al. 2026, Zhang et al. 2026]. To compare, we use Kendall's Tau-b correlation measure, as it is widely used in influential node identification works. The strength of the Kendall's Tau correlation (τ) between these vectors serves as a quantitative measure of our model's fidelity to the underlying network dynamics.

[13]The edge percentage relative to a complete graph with the same number of nodes.

5. Results

Regarding quantitative results, the Adaptive method showed a better overall correlation than the Global method, which also performed better than the Naive method. Figure 1 shows this result across the three aforementioned graph classes, while Figure 2 shows a scatter distribution and a fitted regression across four network densities.

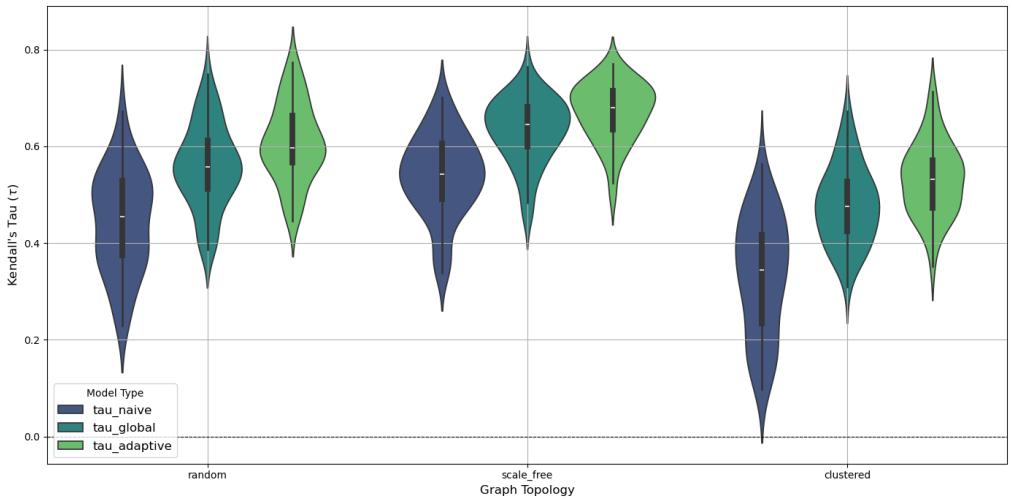


Figure 1. Kendall's tau correlation from the three methods (respectively, for each column, Naive, Global, and Adaptive) across all three graph classes. The proposed methods have better overall correlation than the Naive (uniformly weighted) method.

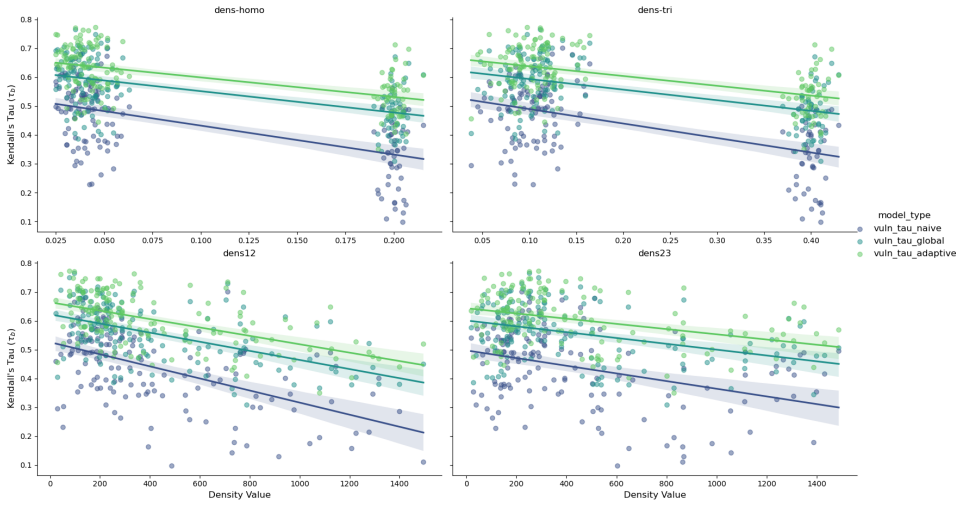


Figure 2. Kendall's tau correlation from the three methods across all four possible densities defined in Table 1. Each colored point represents one of the 150 synthetic graphs. The proposed methods have better overall correlation than the Naive (uniformly weighted) method.

Regarding qualitative results, Figure 3 shows box plots of both measures described in 4.3.1. It shows that all three methods exhibit similar eigenvector fidelity behavior, while the Naive method performs better in terms of threshold fidelity.

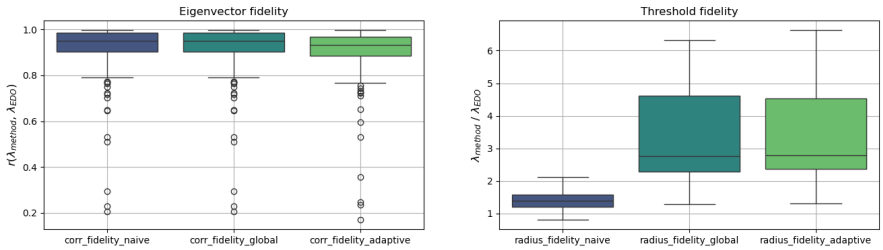


Figure 3. Fidelity across the three graph classes. The left panel shows eigenvector fidelity, while the right panel shows threshold fidelity.

6. Discussions

The Adaptive method is significantly[14] better than the other methods across the three graph categories. Moreover, clustered graphs consistently yield the lowest Kendall τ. This observation is consistent with the behavior of weighted projection on clustered graphs, as such projection accentuates connections among already well-connected nodes. This is characteristic of the rich-club effect, which describes the tendency of high-degree nodes to be more densely interconnected, further strengthening their influence in the network [Irany et al. 2025]. In contrast, scale-free graphs exhibit the least variance, indicating that the preferential attachment topology yields more predictable projection behavior. This finding suggests that hub impact alleviation benefits scale-free networks, including real-world social networks. For both global and adaptive approaches, most Kendall correlations in scale-free graphs fall between 0.6 and 0.8.

This overall outcome is reinforced by Figure 2. Across all density measures in Table 1, the proposed weighted methods achieve higher node rank correlation than the Naive method. The Global method uses a single degree-alleviation parameter for the entire graph, whereas the Adaptive method tunes it per layer. At low to moderate densities, this flexibility yields higher rank correlations with the full tripartite ODE system. However, the regression curve shows some overlap between the Global and the Adaptive method on bipartite densities with higher values. In these scenarios, the degree distribution across tripartite layers becomes uniform, which reduces the advantage of both Global and Adaptive methods. This happens because both methods address heterogeneity in degree distributions. Moreover, it also reinforces that condensed bipartite hub regions retain distorted influences on diffusion propagation even after the proposed degree alleviation [Bisanzio et al. 2010]. Therefore, our results indicate this effect persists for tripartite cases with uniform degree distributions.

Figure 3 shows similar interquartile ranges of the epidemic fidelity (left panel) across every graph class, suggesting that outbreak sizes are preserved across the three methods, as the leading eigenvector is preserved regardless of the weighting method. Therefore, all three projection methods can identify spreaders. However, this behavior also occurs with the Naive, implying that this measure cannot discriminate between them based on performance. Nonetheless, Figure 3 also shows that the Naive projection has more threshold fidelity (right panel) values close to 1, suggesting that spectral radius drifts away from the one on the tripartite structure when accounting for degree hetero-

[14] Wilcoxon signed-rank, $p < 0.001$, Holm-corrected.

geneity. This is consistent with prior work (mentioned in Section 2) suggesting that degree-alleviation weighting shifts the spectral radius away from the original system's value. On the other hand, the spectral radius scales with graph size, and the projected unipartite graph has fewer nodes than the tripartite system. Thus, the Naive method's apparent advantage on this measure should be treated as a preliminary observation rather than a confirmed result.

These results confirm the work of [Lee et al. 2021] by highlighting diffusion distortion by unipartite projections. However, our work also shows that weighted projections can improve influence rank correlation over Naive aggregation on a static tripartite SIR system. At the same time, the Naive method's advantage on threshold fidelity indicates that degree alleviation weighting introduces a spectral bias that unweighted projection avoids.

6.1. Parameter analysis

Table 2 presents the parameters for the tripartite ODE and the three proposed methods. The tripartite ODE system uses seven parameters and requires solving $|N| = |N_1| + |N_2| + |N_3|$ equations, where $|N_i|$ denotes the number of nodes in the i-th layer. In comparison, the proposed methods require at most four parameters and project SIR onto $|N_1|$ equations. Alleviation parameters (α) are estimated once per graph structure, so only two parameters are fitted to the epidemic data.

Table 2. Parameters are listed for the tripartite ODE set and each proposed method according to Equations 1, 3, 4, and 5.

Method	Parameters
Tripartite ODE	$\beta_{12}, \beta_{21}, \beta_{23}, \beta_{32}, \gamma_1, \gamma_2, \gamma_3$
Naive method	$\beta_{proj}, \gamma_{proj}$
Global method	$\beta_{proj}, \gamma_{proj}, \alpha_{global}$
Adaptive method	$\beta_{proj}, \gamma_{proj}, \alpha_2, \alpha_3$

Furthermore, Figure 4 illustrates α_{Global} α_2 and α_3 in all three classes. In this context, it shows how individual graphs can affect alpha. These values were fitted as described in Section 4. Moreover, Figure 5 shows landscapes of the parameters α_2 and α_3 along with the average τ and eigenvector fidelity per 50 graphs (for each graph class). It represents how different alpha values can impact other measures.

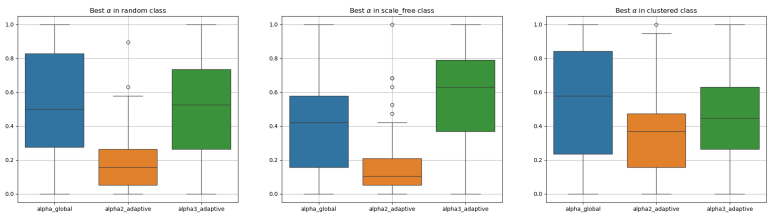


Figure 4. Best individual parameters for each network. From left to right, these panels represent random, scale-free, and clustered network classes, respectively.

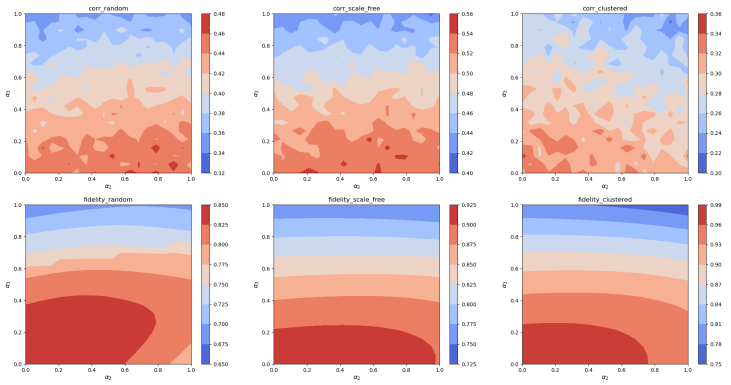


Figure 5. Alpha combination landscape from the Adaptive method, according to the exhaustive fit. First row shows τ over the surface, while the second row shows the eigenvector fidelity defined in 4.3.1.

As shown in Figure 4, the Global parameter shows a similar interquartile distance to the third-most layer parameter of the Adaptive method (α_3), while α_2 consistently has lower values than both. This indicates that diffusion is individually more sensitive to hubs at layers farther from the target layer. Moreover, its sensitivity is reflected in α_{global} values. This demonstrates the Adaptive method's advantage over the Global approach, since the best individual α_2 values are lower. The Global method, by contrast, forces this parameter to over-alleviate layer 2, which results in worse performance. However, according to Figure 5, the Adaptive method achieves better τ when α_3 is lower, on average, across 50 graphs per graph class. Best average fidelity regions are upper-bounded around $\alpha_3 < 0.4$ on random graphs and $\alpha_3 < 0.2$ on scale-free and clustered graphs, while α_2 range is wider in all cases. This suggests that choosing an inadequate α_3 can reduce performance on average across the graphs. Moreover, the eigenvector fidelity landscape exhibits smoother curves and well-defined regions, suggesting it is more sensitive to parameter choice than rank correlation τ. Both figures complement each other, as they suggest that α_3 is the coarse-grained influential parameter on average. In contrast, α_2 stands as a finer-grained individual influence parameter. Therefore, an Adaptive model could be tuned by choosing a relatively low α_3 and adjusting α_2 based on the graph's specific topology.

7. Conclusions

This work proposed a weighted metapath-based SIR model for a tripartite network, projecting the multipartite network onto a single weighted unipartite graph to simulate standard SIR. We introduced two parameterized approaches to construct the weighting matrix. After evaluating 150 synthetic networks, the results suggest a trade-off between the Naive, unweighted projection and the Adaptive degree-alleviating projection. The former better preserves the epidemic threshold and reduces bias towards degree homogeneity, while the latter yields improved node rank correlations. In contrast, the Global projection method, which applies a single degree-alleviation parameter uniformly, falls between the other two. Thus, these findings suggest that there is no single projection strategy ideal for every diffusion model quality metric.

Given the preliminary nature of this study, we identify at least four directions for future work. First, α parameters are currently optimized by grid search, given access to the ground truth. Therefore, further experimenting with held-out optimization is required. Second, the threshold fidelity measure — defined as the spectral radius ratio between the projected and original graphs — may be affected by differences in network size. Therefore, applying a size-corrected comparison, such as computing R_0 via the next-generation matrix [Diekmann et al. 2009], is necessary to assess potential size bias in the results. Third, the method should be evaluated on real-world multipartite datasets, such as heterogeneous information networks, to determine whether results from synthetic graphs generalize to natural topologies. Lastly, the method should be tested on larger graphs, since this evaluation is currently limited to relatively small synthetic networks, and the scalability of the proposed framework remains to be studied.

Acknowledgements

This study was financed in part by the Coordenação de Aperfeiçoamento de Pessoal de Nível Superior – Brasil (Capes) – Finance Code 001.

Disclosure of interests

The authors have no competing interests to declare that are relevant to the content of this article.

References

Bisanzio, D., Bertolotti, L., Tomassone, L., Amore, G., Ragagli, C., Mannelli, A., Giacobini, M., and Provero, P. (2010). Modeling the Spread of Vector-Borne Diseases on Bipartite Networks. *PLOS ONE*, 5(11):e13796.

Castillo-Garsow, C. W. and Castillo-Chavez, C. (2020). A tour of the basic reproductive number and the next generation of researchers. In *An introduction to undergraduate research in computational and mathematical biology: from birdsongs to viscosities*, pages 87–124. Springer.

Diekmann, O., Heesterbeek, J. A. P., and Roberts, M. G. (2009). The construction of next-generation matrices for compartmental epidemic models. *Journal of the royal society interface*, 7(47):873.

Granovetter, M. (1978). Threshold models of collective behavior. *American Journal of Sociology*, 83(6):1420–1443.

Guo, Q., Ye, M.-M., and Liu, J.-G. (2026). Identifying important nodes based on local and global information. *Expert Systems with Applications*, 296:129192.

Gómez-Gardeñes, J., Latora, V., Moreno, Y., and Profumo, E. (2008). Spreading of sexually transmitted diseases in heterosexual populations. *Proceedings of the National Academy of Sciences*, 105(5):1399–1404.

Irany, F. A., Kundu, T., Sarakar, S., Mukherjee, A., and Bhowmick, S. (2025). Centrality resilience in complex networks. In Lees, M. H., Cai, W., Cheong, S. A., Su, Y., Abramson, D., Dongarra, J. J., and Sloot, P. M. A., editors, *Computational Science – ICCS 2025*, pages 36–45, Cham. Springer Nature Switzerland.

Kempe, D., Kleinberg, J., and Tardos, E. (2003). Maximizing the spread of influence through a social network. In *Proceedings of the Ninth ACM SIGKDD International Conference on Knowledge Discovery and Data Mining*, KDD '03, page 137–146, New York, NY, USA. Association for Computing Machinery.

Kermack, W. O. and McKendrick, A. G. (1927). A contribution to the mathematical theory of epidemics. *Proceedings of the Royal Society of London. Series A, Containing Papers of a Mathematical and Physical Character*, 115(772):700–721.

Kovács, I. A., Luck, K., Spirohn, K., Wang, Y., Pollis, C., Schlabach, S., Bian, W., Kim, D.-K., Kishore, N., Hao, T., et al. (2019). Network-based prediction of protein interactions. *Nature communications*, 10(1):1240.

Lee, H. A., Alves, L. G. A., and Nunes Amaral, L. A. (2021). Spreader events and the limitations of projected networks for capturing dynamics on multipartite networks. *Physical Review E*, 103(2):022320.

Newman, M. (2018). *Networks*. Oxford University PressOxford, 2 edition.

Pastor-Satorras, R. and Vespignani, A. (2001). Epidemic dynamics and endemic states in complex networks. *Phys. Rev. E*, 63:066117.

Santos, A., Moura, J. M. F., and Xavier, J. (2013). Epidemics in Multipartite Networks: Emergent Dynamics. arXiv:1306.6812 [cs.SI].

Sun, Y. and Han, J. (2012). *Mining Heterogeneous Information Networks: Principles and Methodologies*. Morgan & Claypool Publishers.

Takko, T., Bhattacharya, K., and Kaski, K. (2023). Modelling exposure between populations using networks of mobility during COVID-19. *Frontiers in Physics*, 11.

Wang, J., Lin, B., Du, Z., Li, P., and Xu, X.-K. (2025). Six-Degree Gravity Centrality for Detecting Influential Nodes in Networks. *Chinese Physics B*.

Xu, W., Lu, Z., Wang, C., Han, Y., and Yu, Y. (2025). Dynamic Analysis of a Fractional-Order Model for Vector-Borne Diseases on Bipartite Networks. *Fractal and Fractional*, 9(11):742.

Zhang, H., Dong, L., Xu, W., Wu, Y., Jin, X., Xie, X., and Zhang, H. (2026). Influential node identification via network embedding and structural feature fusion. *Chaos, Solitons & Fractals*, 208:118092.

Zheng, W., Shi, W., Fan, T., and Lü, L. (2025). Weighted cycle-based identification of influential node groups in complex networks. arXiv:2503.11974 [cs].